Applied Catalysis A: General 468 (2013) 260–268

Contents lists available at ScienceDirect

Applied Catalysis A: General

journal homepage: www.elsevier.com/locate/apcata

# Facile synthesis of $CeO_2$-supported gold nanoparticle catalysts for selective oxidation of glycerol into lactic acid

Pandian Lakshmanan[a], Pravin P. Upare[a,b], Ngoc-Thuc Le[a,b], Young Kyu Hwang[a,b,*], Dong Won Hwang[a,b], U-Hwang Lee[a], Hyung Rok Kim[a,b], Jong-San Chang[a,b,c,**]

[a] Catalysis Center for Molecular Engineering, Korea Research Institute of Chemical Technology (KRICT), 141 Gajeong-Ro, Yuesong, Daejeon 305-600, Republic of Korea
[b] Department of Green Chemistry, University of Science and Technology (UST), 217 Gajeong-Ro, Yuseong, Daejeon 305-350, Republic of Korea
[c] Department of Chemistry Sungkyunkwan University, Suwon 440-476, Republic of Korea

ARTICLE INFO

*Article history:*
Received 15 April 2013
Received in revised form 7 August 2013
Accepted 28 August 2013
Available online xxx

*Keywords:*
Biomass
Glycerol oxidation
Lactic acid
Gold nanoparticles
Cerium oxide
Chemical-reduction

ABSTRACT

This study explores a new synthetic route toward $CeO_2$-supported gold nanoparticles catalysts (1, 3, and 5 wt.% Au) and their catalysis of the oxidation of glycerol at atmospheric pressure. Gold was loaded on a hydrothermally synthesized nanocrystalline $CeO_2$ support (~8 nm) via deposition-precipitation with urea (DPU). To obtain cerium oxide-supported gold nanoparticles, thermal reduction at 300 °C under flowing $H_2$ is currently popular. However, this method invariably forms small gold particles (<5 nm) even with higher gold loading. In the present study, $Au/CeO_2$ catalysts prepared by DPU were reduced via a new method: chemical reduction with glycerol (CRG). Interestingly, the reduction of a gold-urea complex supported on ceria occurs at 25 °C, and the gold nanoparticles grow slowly. The resultant chemically reduced samples were compared with their hydrogen-reduced counterparts. The CRG method primarily generated gold particles with larger average sizes than the $H_2$ reduction method. Importantly, the CRG route enabled variation of the average gold nanoparticle size without requiring any other reagent, which is particularly advantageous for the $Au/CeO_2$ system. The efficiency of these catalysts toward the aerobic oxidation of glycerol was tested. Accordingly, the selective oxidation of glycerol into lactate can be effectively catalyzed by $Au/CeO_2$ catalysts at atmospheric pressure. The chemically reduced samples show increased lactate selectivity than the hydrogen-reduced samples due to the larger size of the gold particles.



## 1. Introduction

The use of bio-renewable resources for the production of chemicals continues to attract significant research attention to support sustainable development. Glycerol is a particularly intriguing reagent since it is a major co-product of biodiesel production. The oxidation of glycerol leads to the formation of a number of valuable oxygenated compounds such as glyceric acid, lactic acid, dihydroxyacetone, hydroxypyruvic acid, glycolic acid, oxalic acid, and tartronic acid. Hence, control of product selectivity is crucial. Conversion of glycerol into lactic acid is very significant from the perspective of the applications of lactic acid: Lactic acid is the building block for the synthesis of polylactic acid (PLA) [1], which is involved in the production of biodegradable plastics and biocompatible medical materials [2–5]. Selective oxidation of glycerol primarily using supported noble metal nanoparticles such as Pd, Pt, and Au with molecular oxygen [6–14] has been extensively studied, mainly for glyceric acid production. Previous studies showed that lactic acid can be generated from glycerol through a heterogeneous catalysis process. Different approaches including a hydrothermal reaction [15–17], hydrogenolysis [18,19], and catalytic selective oxidation [3,20–31] have been applied for the synthesis of lactic acid from glycerol. Compared to the hydrothermal and hydrogenolysis methods [15–19], catalytic selective oxidation allows the reaction to be performed under milder reaction conditions [32] with supported gold catalysts.

The problem in the production of lactic acid from glycerol via a selective oxidation process is that the glyceraldehyde intermediate and its isomer, dihydroxyacetone, are susceptible to further oxidation [3,20,21]. This has been problematic in previous studies, resulting in the formation of primarily glyceric acid without

* Corresponding author at: Catalysis Center for Molecular Engineering, Korea Research Institute of Chemical Technology (KRICT), 141 Gajeong-Ro, Yuesong, Daejeon 305-600, Republic of Korea. Tel.: +82 42 860 7680; fax: +82 42 860 7676.
** Corresponding author at: Catalysis Center for Molecular Engineering, Korea Research Institute of Chemical Technology (KRICT), 141 Gajeong-Ro, Yuesong, Daejeon 305-600, Republic of Korea. Fax: +82 42 860 7676.
*E-mail addresses:* ykhwang@krict.re.kr (Y.K. Hwang), jschang@krict.re.kr (J.-S. Chang).

0926-860X/$ – see front matter © 2013 Elsevier B.V. All rights reserved.
http://dx.doi.org/10.1016/j.apcata.2013.08.048

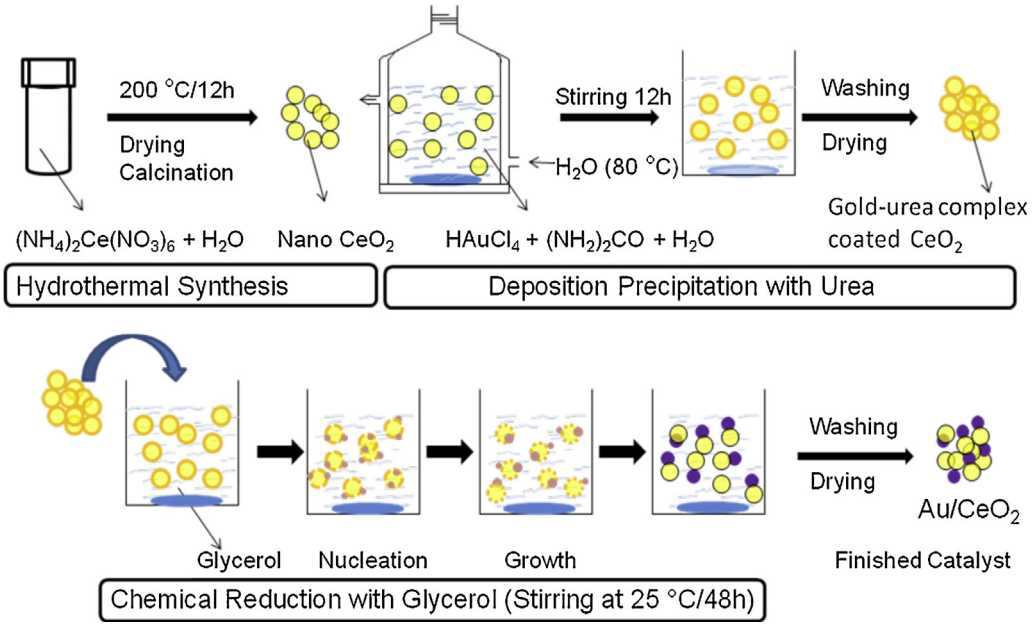


**Scheme 1.** Schematic illustration of the synthesis of $Au/CeO_2$ catalysts by chemical reduction with glycerol.

any significant formation of lactic acid in most of the cases [9–16]. Product selectivity during glycerol oxidation is strongly influenced by the size of the gold particles and reaction conditions [26,33–35]. With Au/C catalysts, larger particles (>20 nm) imparted improved selectivity to glyceric acid compared to gold particles with an average size of 6 nm [26]. For gold particles, the activity toward the formation of lactate from propylene glycol increased with decreasing particle size (70 °C, 2 atm $O_2$, 1 equiv. NaOH), whereas with carbon-supported gold, the maximum activity (100% conversion, selectivity was not mentioned) was achieved with a mean gold particle diameter of 7–8 nm [33].

The higher catalytic activity of the carbon-supported gold particles toward the conversion of glycerol to glyceric acid was attributed to the small size of the Au nanoparticles, which were supported on anionic exchange resins (50 °C, 3 atm $O_2$, 4 equiv. NaOH) [34]. By tuning the metal particle size from 2 to 16 nm, a progressive decrease in activity and simultaneous increase in selectivity for sodium glycerate production was observed [35]. Baiker et al. studied the catalytic activity of $Au/CeO_2$ with different sizes of gold particles (ranging from 1.5 to 12 nm) on the aerobic oxidation of benzyl alcohol. Accordingly, optimal activity was observed for catalysts with medium particle sizes (~6.9 nm), whereas both smaller and larger particles showed inferior activity (100 °C, 1 atm $O_2$, no base, toluene/mesitylene as solvent) [36].

Hydrogen-reduced $Au/CeO_2$ samples invariably form smaller gold nanoparticles (<5 nm) regardless of the gold loading [37,38]. Since smaller gold particles favor the formation of glyceric acid, not much attention was paid to $Au/CeO_2$ for the conversion of glycerol to lactic acid. Herein, we report the facile synthesis of nanoparticle $Au/CeO_2$ catalysts with varying average gold particle sizes and their efficiency toward the catalysis of the selective aerobic oxidation of glycerol to lactic acid at atmospheric pressure. The synthesis of $Au/CeO_2$ catalysts with different average gold particles was accomplished using the glycerol-based chemical reduction protocol (CRG). The efficiency of this method was examined with three different gold loadings. The synthesized gold catalysts were characterized via elemental analysis, UV–vis spectroscopy, X-ray diffraction, and high-resolution transmission electron microscopy (HR-TEM).

## 2. Experimental

### 2.1. Hydrothermal synthesis of nanocrystalline ceria support

The appropriate quantity of cerium ammonium nitrate salt (Aldrich, 98.5%) to achieve a concentration of 0.1 M was dissolved in deionized water and stirred vigorously for 30 min. This solution was then poured into an autoclave and treated hydrothermally at 200 °C for 12 h (Scheme 1). The resultant precipitates were separated by centrifugation, washed with deionized water, dried in an oven at 80 °C for 2 h, and calcined at 450 °C for 3 h under flowing air.

### 2.2. Au-loading by deposition precipitation using urea (DPU)

The calcined ceria was dispersed in distilled water and maintained at 80 °C. A solution of $HAuCl_4{\cdot}4H_2O$ was added followed by the addition of urea (Scheme 1); the resulting mixture was stirred at 80 °C for 12 h. Centrifugation was performed to isolate the solid, which was washed thrice with distilled water to remove chlorides and then dried in a desiccator.

### 2.3. Reduction of gold catalysts via chemical reduction with glycerol (CRG)

In a typical process, the $Au/CeO_2$ samples obtained via the DPU method were mixed in a beaker with the appropriate quantity of glycerol and stirred at ambient temperature for 48 h (Scheme 1, second step). The reduced solid catalysts were separated from glycerol via centrifugation and then washed thrice with deionized water to remove the glycerol. The sample was directly transferred into the reaction mixture for glycerol oxidation.

### 2.4. Characterization

Chemical analyses were performed via inductively coupled plasma atomic emission spectroscopy (ICP-AES) using a Thermo Scientific ICAP 6500 instrument. The Au loadings are expressed as wt.%. X-ray diffraction (XRD) analysis was performed on a Rigaku D/MAX-2200V diffractometer (Cu Kα). TEM analysis was

performed using a TECNAI G2 microscope. UV–vis spectroscopic measurements were carried out using a SHIMADZU UV-1800 instrument.

### 2.5. Catalytic testing

Reactions were carried out in a three-necked round-bottom flask (100 mL) equipped with air flow at atmospheric pressure under vigorous stirring at 90 °C. The products were analyzed via high-pressure liquid chromatography (HPLC) using an Alltech OA-1000 column (300 mm × 6.5 mm) with 0.1% $H_3PO_4$ solution as the eluent. For the HPLC analyses, 0.5 mL of the reaction mixture was diluted to a total volume of 5.0 mL with the eluent. The products were identified by UV (210 nm) and refractive index detectors by comparing them to the original samples. Glycerol appears only in a refractive index detector giving a strong signal. For example, glycerol was determined using the refractive index detector, while lactic acid was determined using UV detector (Figs. S1 and S2).

The conversion of glycerol, selectivity to product, and carbon balance were calculated according to Eqs. (1)–(3), respectively.

$$\text{Conversion (\% mole)} = \frac{\text{Moles of glycerol converted}}{\text{Moles of glycerol initial}} \times 100 \quad (1)$$

$$\text{Selectivity (\% mole)} = \frac{\text{Moles of product formed}}{\text{Total moles of } C_1 + C_2 + C_3 \text{ products formed}} \times 100 \quad (2)$$

$$\text{Carbon balance (\% mole)} = \frac{3M_{C_3} + 2M_{C_2} + M_{C_1}}{3M_{CC}} \times 100 \quad (3)$$

where $M_{CC}$ is total the moles of glycerol converted, $M_{C_3}$ is the moles of the $C_3$ products (lactic, glyceric and tartronic acids), $M_{C_2}$ is the moles of $C_2$ products (glycolic and oxalic acids), and $M_{C_1}$ is the moles of $C_1$ product (formic acid), respectively.

## 3. Results and discussion

### 3.1. Characterization of $CeO_2$-supported gold catalysts

The nanocrystalline ceria support synthesized via the hydrothermal method exhibited a surface area of 120 $m^2/g$ determined from the $N_2$ isotherm. Elemental analyses via ICP-AES showed gold loadings of 0.95, 2.74, and 4.59 wt.%, which are close to the nominal loadings of 1, 3, and 5 wt.%, respectively. Fig. 1 shows the presence of $CeO_2$ with distinguishable peaks that indicate dominant (1 1 1), (2 0 0), (2 2 0), and (3 1 1) diffraction patterns, suggesting a cubic structure of calcium fluorite ($CaF_2$; JCPDS 35-0816). The average particle size, which was calculated using the Scherrer equation, suggests that the ceria nanoparticles are ~8 nm. Powder XRD patterns of the 1% Au/$CeO_2$ samples after chemical reduction with varying amounts of glycerol are presented in Fig. 1a. The first line (i) in Fig. 1a corresponds to the sample reduced by thermal treatment at 300 °C under a hydrogen flow. As the gold particles are very small, the XRD pattern does not exhibit the diffraction pattern of gold. The other lines in Fig. 1a correspond to the samples reduced by glycerol with catalyst/glycerol weight ratios of 0.002, 0.005, 0.01, 0.02, and 0.04. As is evident in Fig. 1a, these XRD patterns closely resemble that of the hydrogen-reduced sample and the gold diffraction patterns are not visible. The hydrogen-reduced sample is dark brown, while the glycerol-reduced samples are violet-brown; this color difference is indicative of the differences in the average size of the gold particles. However, the XRD patterns are only slightly different at the 2$\theta$ value of 38.2°, which corresponds to the (1 1 1) Bragg reflection of the gold nanoparticles. To display the changes of the

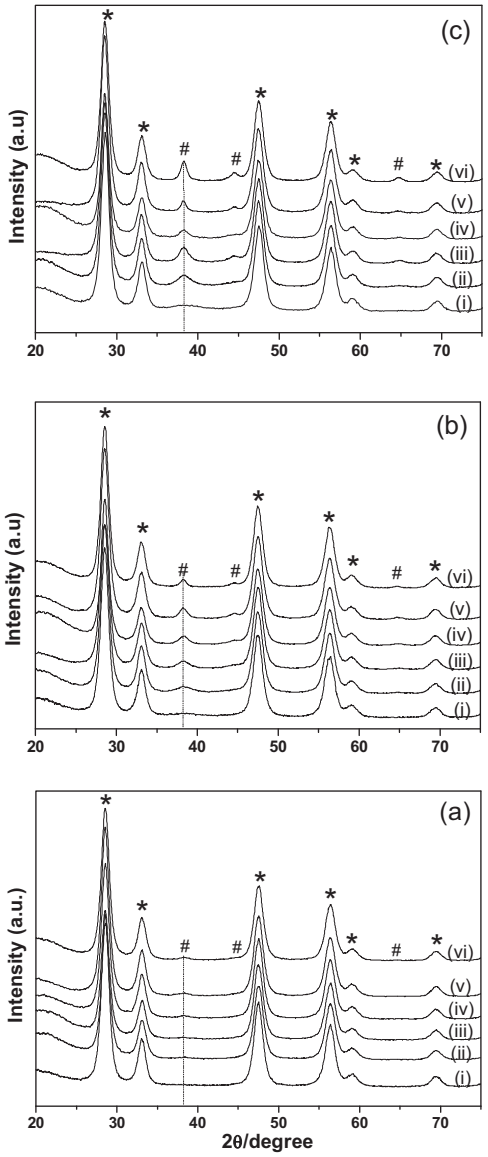


**Fig. 1.** XRD patterns of Au/$CeO_2$ catalyst at different concentration of Au. (a) 0.95 wt.% Au/$CeO_2$, (b) 2.74 wt.% Au/$CeO_2$ and (c) 4.59 wt.% Au/$CeO_2$ by $H_2$-reduction ((i) line) and glycerol reduction with catalyst to glycerol weight ratios of 0.002, 0.005, 0.01, 0.02, and 0.04, respectively (from (ii) to (vi) lines). * and # denoted $CeO_2$ and Au phases, respectively.

sizes of the gold nanoparticles, an expansion of the 2$\theta$ range of 35–45° is shown in Fig. 2. It is evident that the widths of the Bragg reflections for the glycerol-reduced samples gradually decrease as the intensity increases. By comparing the broadening of the curves, it can be inferred that the glycerol-reduced samples ((ii) to (vi) lines) contain larger gold nanoparticles than the hydrogen-reduced sample ((i) line) and that the diameter of the gold particles is dependent on the catalyst/glycerol ratio.

The XRD results for 3% Au/$CeO_2$ are depicted in Fig. 1b. Again, the hydrogen-reduced 3% Au/$CeO_2$ ((i) line) does not exhibit gold peaks. The (ii) line of Fig. 1b shows a significant increase in the intensity of Au (1 1 1) peak in comparison to that of the hydrogen-reduced sample. This clearly shows that the average gold particle size of the samples prepared via CRG is larger than that of the hydrogen-reduced samples. With increasing catalyst/glycerol ratio, a progressive sharpening of the Au (1 1 1) peak is evident. In contrast to the hydrogen-reduced sample, the (1 1 1) Bragg reflection from the gold nanoparticles at the 2$\theta$ value of 38.2° is clearly

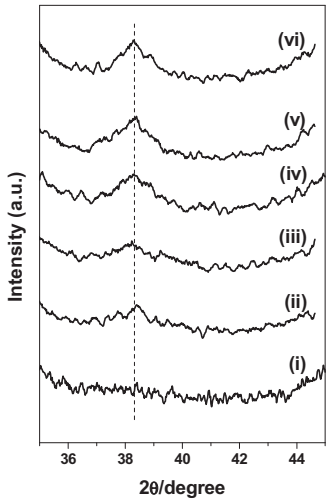


**Fig. 2.** Focused view of XRD patterns of 0.95 wt.% $Au/CeO_2$ sample in the two theta range 35–45° by $H_2$-reduction ((i) line) and glycerol reduction with catalyst to glycerol weight ratios of 0.002, 0.005, 0.01, 0.02, and 0.04, respectively (from (ii) to (vi) lines).

observed for all glycerol-reduced samples. As determined from the broadening of the (1 1 1) reflection in the XRD patterns, the estimated gold particle sizes are plotted in Fig. 3a. As the catalyst/glycerol ratio increases, the FWHM values gradually decrease (not shown) and the estimated average gold particle sizes gradually increase. Accordingly, the hydrogen-reduced sample is dark brown, while the glycerol-reduced samples are violet-brown.

The observed variation of the average gold particle size with the catalyst/glycerol ratio was further confirmed by reducing the

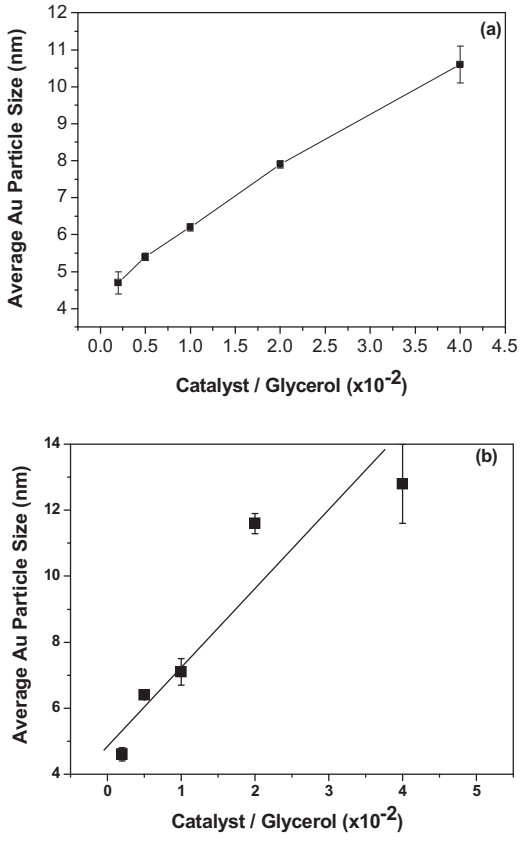


**Fig. 3.** Variation of average gold particle size with catalyst to glycerol ratio: (a) 2.74% $Au/CeO_2$ and (b) 4.59% $Au/CeO_2$.

5% $Au/CeO_2$ catalysts (Fig. 1c). The hydrogen-reduced sample is represented by the first line (i) in Fig. 1c: Compared with 1% and 3% $Au/CeO_2$, the (1 1 1) Bragg reflection from the gold nanoparticles in 5% $Au/CeO_2$ is more intense, but still very broad. On the other hand, the XRD results for glycerol-reduced 5% $Au/CeO_2$ clearly show a gold nanoparticle (111) Bragg reflection peak at the $2\theta$ value of 38.2°. The estimated average gold particle sizes are plotted against the catalyst/glycerol ratio in Fig. 3b. These results show that the average gold particle size increases with increasing catalyst/glycerol ratio. In fact, the colors of the 5% $Au/CeO_2$ catalysts vary significantly: With increasing catalyst/glycerol ratio, the colors varied from light-brown, dark brown, violet, magenta, pink, to gray over time, which reflect the growth of the gold nanoparticles.

During the chemical reduction process, we observed changes in the colors of the $Au/CeO_2$ samples. UV–visible spectroscopy is one of the few effective methods for investigating modifications of the physical or chemical properties of supported gold catalysts. A strong absorbance in the visible region around 540 nm is due to excitation of the surface plasmon vibrations of Au nanoparticles [39–42]. Fig. 4a shows the spectra recorded for 1% $Au/CeO_2$ samples reduced by either hydrogen or different amounts of glycerol. The first line (i) from the bottom shows that the spectrum of the hydrogen-reduced sample is featureless, while the (ii) and (iii) lines also do not exhibit significant absorbance. However, the samples with higher catalyst/glycerol ratios exhibit a gold plasmon resonance (PR) band at 550 nm; the intensity of the band increases from the (iv) to the (vi) line. These results correlate with the XRD results of the corresponding samples. If the gold particles are significantly smaller (<10 nm) than the wavelength of light (300–800 nm), the plasmon band is not dependent on the particle size because it is dipolar-type plasmon resonance [41–45]. Hence, the differences in the PR peak shape could be related to the shape/surface morphology of the formed gold nanoparticles. It has been mentioned that, based on the broadening of the Bragg reflection at the $2\theta$ value of 38.2°, the sizes of the gold particles vary with the catalyst/glycerol ratio. Therefore, the slight differences in the shape of the plasmon resonance band of the glycerol-reduced samples ((ii) to (vi) lines in Fig. 4a) suggest that the catalyst/glycerol ratio could affect the shapes of the gold nanoparticles formed on the ceria surface. During synthesis of the catalyst, an increased catalyst/glycerol ratio results in less separation of the catalyst particles, which increases the potential for the growth of the nanocrystals by an aggregative mechanism. In contrast, if there is a large amount of glycerol, the frequency of collisions between the ceria nanoparticles should decrease due to their increased separation thereby reducing the growth of gold nanoparticles. To verify this hypothesis, we performed the CRG process by thoroughly mixing the 5% $Au/CeO_2$ sample with glycerol (30 min vigorous stirring) and then stopping the stirring and letting the reaction stand for the remainder of 48 h. The resultant sample was violet ($D_{Av.}$ Au ~6 nm) in contrast to the sample obtained with continuous stirring for 48 h, which appears gray ($D_{Av.}$ Au >15 nm). This indicates that effective collision between ceria particles is important for the growth of gold nanoparticles supported on ceria during the CRG process. The shape of the prepared gold nanoparticles also varies, as is evident from the changes in the PR bands of the gold nanoparticles in their UV–vis spectra.

The hydrogen-reduced 3% $Au/CeO_2$ sample also exhibits a featureless spectrum ((i) line, Fig. 4b). In contrast, the glycerol-reduced sample (catalyst/glycerol weight ratio of 0.002, (ii) line) shows a clear absorbance at ~550 nm. Upon increasing the catalyst/glycerol weight ratio, a red shift is noted up to line (iv). Further increasing the catalyst/glycerol ratio leads to broadening of this band and gains in the absorbance at longer wavelengths (~700 nm), which implies further changes in the sizes and shapes of the gold nanoparticles. An additional band at ~710 nm has been used as an indicator of the

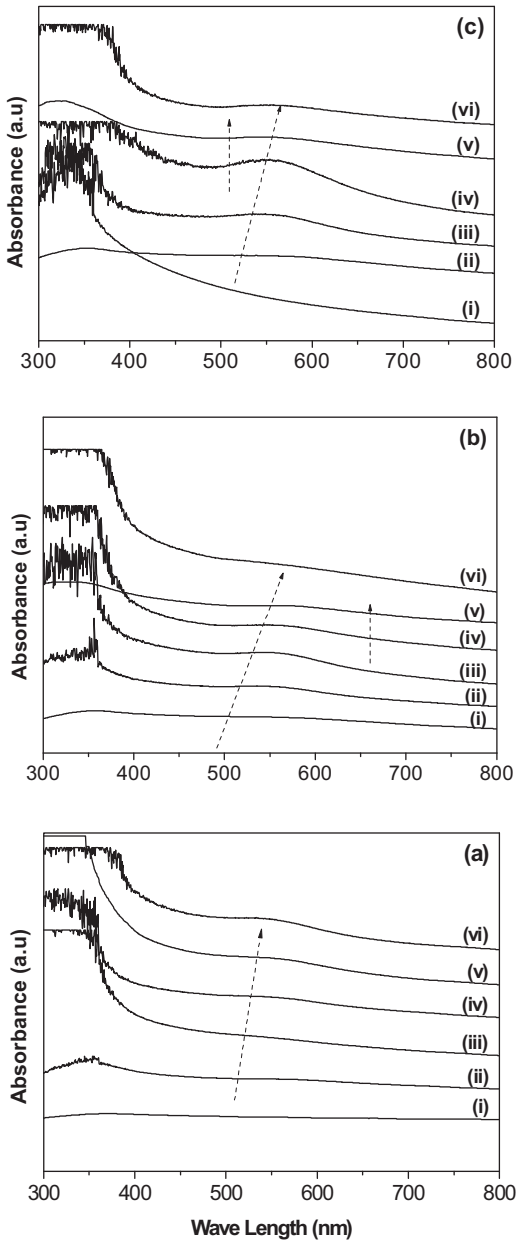


**Fig. 4.** UV–vis absorption spectra of $CeO_2$-supported gold nanoparticles: (a) 0.95% $Au/CeO_2$, (b) 2.74% $Au/CeO_2$ and (c) 4.59% $Au/CeO_2$. The first line (i) from the bottom corresponds to the samples reduced by $H_2$ and all other lines (ii–vi) correspond to the samples reduced by glycerol with catalyst to glycerol weight ratios of 0.002, 0.005, 0.01, 0.02, and 0.04, respectively.

extent of aggregation of nanoparticles and can be attributed to the excitation of longitudinal surface plasmon vibrations due to close-packing of gold nanoparticles [46–48]. Careful comparison of the spectra of the glycerol-reduced 3% $Au/CeO_2$ samples show that the absorbance is slightly higher around 700 nm (indicated by arrow) for samples with a higher catalyst/glycerol ratio ((v) and (vi) lines); however, there is no significant band. This indicates that varying the amount of glycerol may slightly change the average particle size, but there is no significant aggregation. It is worth noting the color differences: The sample pertaining to the (iv) line appears gray, which indicates that it contains larger gold nanoparticles.

Fig. 4c shows the UV–vis spectra of the 5% $Au/CeO_2$ samples. The hydrogen-reduced sample exhibits a very broad line shape, while the glycerol-reduced samples clearly show absorbance due to gold surface plasmon resonance. The sample reduced with a

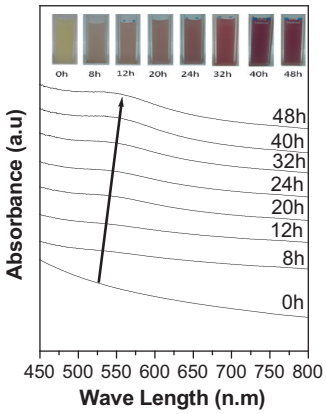


**Fig. 5.** Time-dependant UV–vis spectroscopy study during the chemical reduction process with 4.59% $Au/CeO_2$.

catalyst/glycerol ratio of 0.002 ((ii) line in Fig. 4c) displays a band centered at ~550 nm. With increasing catalyst/glycerol ratio, the absorbance increases significantly and undergoes a red shift ((iii) and (iv) lines). Further increasing the catalyst/glycerol ratio leads to drastic changes in the line shape including broadening and increased absorption in the longer wavelength region. However, no significant band at ~700 nm is evident, which suggests that, despite the increased average size, very large aggregated gold particles do not form. As mentioned earlier, the significant differences in the absorbance of the (ii) to (iv) lines are not related to size increases since the wavelength of light used in the present study (i.e., 450–800 nm) is larger than the sizes of the gold particles. Hence, such significant differences could be related to significant shape variations of the gold nanoparticles since the gold loading is significantly higher. This conclusion is strongly supported by the XRD results. Within the limitations of the XRD results, there is a significant difference in the average sizes of the glycerol-reduced samples, which could explain the shape variation and hence the different shapes of the gold plasmon resonance band for each sample. The 5% $Au/CeO_2$ samples clearly show that the CRG technique can form larger gold particles than the hydrogen-reduction technique at 300 °C. The significant differences between the (ii) to (iv) lines also suggest that the amount of glycerol affects the shape and size of the gold particles with a catalyst with fixed gold loading. The results obtained via UV–vis spectroscopy correlate well with the XRD results and the colors of the catalysts.

To optimize the reaction time of the chemical-reduction procedure, time-dependant UV–vis spectroscopy was performed (Fig. 5). The 5% $Au/CeO_2$ sample is initially yellow, which indicates the presence of unreduced gold in the as-prepared DPU sample. At this stage, a UV–vis spectrum was recorded (0 h line). Spectra were then recorded at specific time intervals until a stable gold plasmon resonance band was obtained. At 8 h, the yellow color disappears and the sample shows a featureless UV spectrum. Note that the spectra recorded at 8 h and 12 h resemble those of the hydrogen-reduced samples; this suggests the formation of small gold nanoparticles, which correlates with the light-brown color of the sample. The spectrum recorded at 20 h shows a PR band centered at ~550 nm. Over time, the color of the sample changes from brown to violet. A corresponding red shift in the UV–vis spectra reveals that the shape of the gold nanoparticles changes. After a stable PR band was attained at 48 h, stirring was stopped and the sample was used for the catalytic run. During the chemical-reduction process, aliquots of this sample were removed to examine the gold in the glycerol. The aliquots were centrifuged to separate the liquid and tested for the presence of gold via ICP: Gold was not detected in any of the samples removed at different time intervals. The

combined results of UV–vis spectroscopy, XRD, and colors of the samples clearly show that glycerol acts as a mild reducing agent for gold-ceria DPU samples, resulting in the preparation of ceria-supported gold nanoparticles in an environmentally friendly and facile manner. The use of glycerol to reduce gold provides a single-reagent method for the synthesis of supported gold nanoparticles. A schematic illustration of chemical reduction process is shown in Scheme 1. In the first step of the DPU process, gold is loaded onto the ceria nanoparticles as a gold-urea complex. This as-prepared yellow powder is dispersed in glycerol and stirred for 48 h. After nucleation and growth, the reaction mixture containing the finished catalyst is diluted with excess water and centrifuged to remove glycerol (3 times) and then mixed with the reaction mixture.

A representative HRTEM image of pure ceria support is shown in Fig. 6a. The inter-planar spacing of ~0.3 nm corresponds to the (1 1 1) plane of the fluorite cubic structure of cerium oxide. From the TEM analyses, we determined that the cerium oxide particles have an average size of ~8 nm, which is in good agreement with the particle size measured by XRD. Fig. 6b shows the HRTEM image of glycerol-reduced 5% Au/$CeO_2$, which reveals the presence of Au particles in close contact with $CeO_2$. The inter-planar spacing of $CeO_2$ (~0.3 nm), which corresponds to the (1 1 1) plane of the cerium oxide, could be distinguished from that of Au (~0.21 nm), which corresponds to the (2 0 0) plane of gold. It is known that conventional TEM cannot reveal small gold particles on ceria that has a high surface area [48,49] due to the poor contrast between Au and $CeO_2$ [50,51]. Despite the difficulty of TEM measurement in high magnification, we conducted the TEM analysis in a low magnification to confirm the particle size of Au nanoparticle on $CeO_2$. Fig. 7 shows the low magnification of TEM images and particle size distributions of gold nanoparticles corresponding to the 3% Au/$CeO_2$ (a) and 5% Au/$CeO_2$ (b) samples reduced by glycerol with a catalyst to glycerol ratio of 0.04. The individual particles of Au have spherical shapes and are well dispersed with average sizes of 6–7 nm in 3% Au/$CeO_2$, and 7–8 nm in 5% Au/$CeO_2$, respectively. This result matches well with the particle size measured by XRD in Table 1. From histograms of samples, even in the presence of gold particles

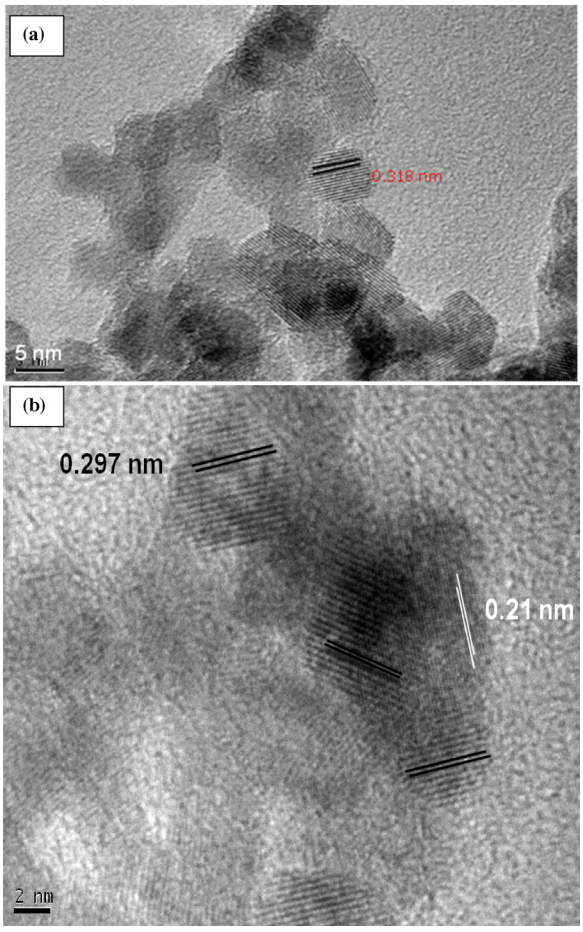


**Fig. 6.** HR-TEM images of (a) pure ceria support and (b) 5% Au/$CeO_2$.

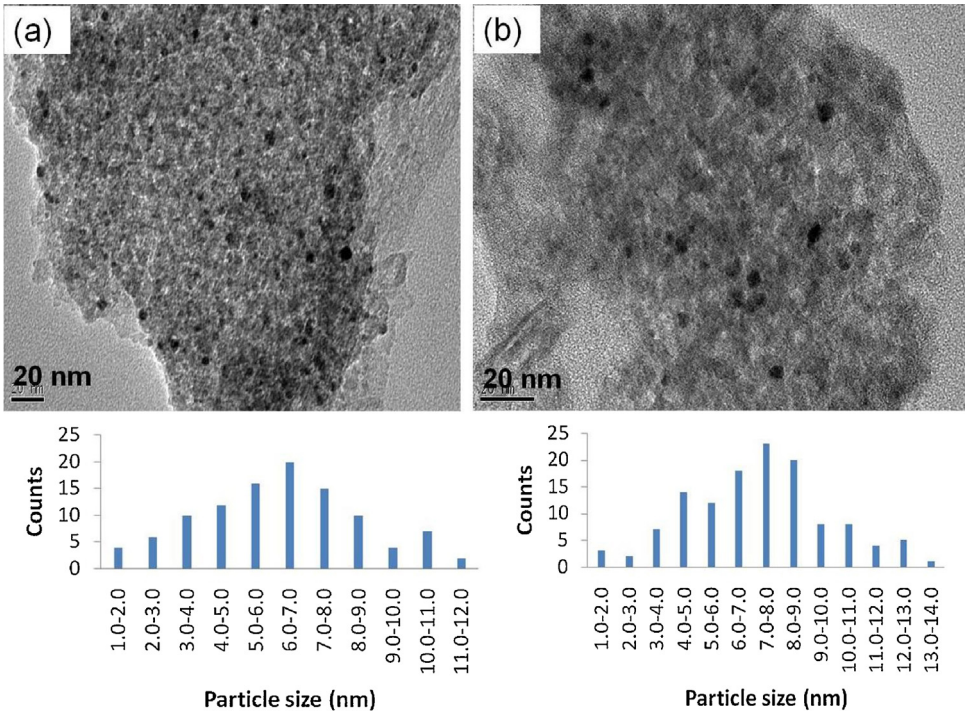


**Fig. 7.** TEM images and particle size distribution of (a) 3% Au/$CeO_2$ and (b) 5% Au/$CeO_2$ samples reduced by glycerol with the catalyst to glycerol ratio of 0.04.

**Table 1**
Product distribution in the oxidation of glycerol using $Au/CeO_2$ catalysts.

| Catalysts | Conv. (%) | Selectivity (%) | | | | | | Particle sizes (nm)[g] |
|---|---|---|---|---|---|---|---|---|
| | | LAC | GLY | TAR | OXA | GLYC | FOR | |
| 1% $Au/CeO_2$[a] | 99.1 | 73.1 | 24.8 | 1.4 | 0.3 | 0.2 | 0.2 | n.d. |
| 1% $Au/CeO_2$[b] | 97.8 | 75.8 | 21.4 | 2.1 | – | – | – | 3.0 |
| 1% $Au/CeO_2$[c] | 98.5 | 77.1 | 19.8 | 1.3 | 0.7 | 0.3 | 0.8 | 4.0 |
| 1% $Au/CeO_2$[d] | 98.0 | 83.0 | 15.7 | 1.1 | 0.2 | – | – | 6.0 |
| 3% $Au/CeO_2$[a] | 98.0 | 73.5 | 22.7 | 2.07 | 1.22 | 0.25 | 0.26 | <5 |
| 3% $Au/CeO_2$[e] | 98.0 | 79.7 | 18.4 | 0.9 | 0.2 | 0.5 | 0.3 | 6.2 |
| 5% $Au/CeO_2$[a] | 98.0 | 72.2 | 24.5 | 2.0 | 0.7 | 0.6 | – | <5 |
| 5% $Au/CeO_2$[f] | 98.0 | 79.0 | 18.3 | 1.0 | 0.2 | 0.6 | 0.8 | 8.2 |

Reaction conditions: temperature of 90 °C, pressure of 1 atm under air with a flow rate of 0.15 L $min^{-1}$, and NaOH/glycerol = 4:1 (mole ratio). n.d.: not determined. LAC: lactic acid; GLY: glyceric acid; TAR: tartronic acid; OXA: oxalic acid; GLYC: glycolic acid; FOR: formic acid. The carbon balance: [a]98%, [b]94%, [c]99%, [d]94%, [e]98%, [f]97%, for hydrogen-reduced 3% $Au/CeO_2$ and 5% $Au/CeO_2$, 93% and 95%, respectively.

[a] $H_2$ reduced samples.

[b–f] Glycerol reduced samples with catalyst to glycerol weight ratios of 0.005 (b), 0.01 (c), 0.02 (d) and 0.04 (e and f), respectively.

[g] Particle size of Au was confirmed by XRD.

with size below 4 nm, it can be seen that majority of the particles lies between 5 nm and 8 nm in particles size. It demonstrates that glycerol reduction can lead to the formation of larger gold particles above 5 nm, which is not possible with the hydrogen-reduced samples.

### 3.2. Catalytic activity toward the selective oxidation of glycerol

The oxidation of glycerol leads to the formation of a mixture of acid products (Table 1). In the present study, lactic (LAC) and glyceric (GLY) acids are the main products, while oxalic (OXA), tartronic (TAR), glycolic (GLYC), formic (FOR), and acetic acids are produced in lesser amounts (see Supporting information for the HPLC chromatographs of a typical reaction mixture (Fig. S1) and the mixtures of authentic compound (Fig. S2)). In the presence of excess base, the reaction proceeds well, while in the absence of base, no reaction occurs. Without the gold catalyst, neither NaOH nor pure ceria support could catalyze the glycerol conversion. These observations are consistent with literature reports [15,32] that gold catalyst, base, and oxygen are required for the oxidation reaction to occur. According to literature, several factors such as gold particle size, nature of the support, and the reaction conditions (i.e., presence/absence of base, metal/glycerol ratio, reaction temperature, and oxygen pressure) influence the catalytic performance (i.e., conversion and selectivity) toward glycerol oxidation reactions. In the present study, the nature of the support and the reaction conditions were held constant. All reactions were carefully performed under identical conditions to validate the comparison. The average sizes of the gold particles were changed by reducing the as-prepared catalysts in different manners. Therefore, we attempt to correlate the catalytic results with changes in the sizes of the gold particles.

In the case of hydrogen-reduced 1% $Au/CeO_2$, the selectivities to lactic acid and glyceric acid were found to be 73.1% and 24.8% respectively (Table 1). In the case of hydrogen-reduced 3% and 5% $Au/CeO_2$ samples, nearly the same values of selectivities were obtained (72.5%, 22.8% for 3% $Au/CeO_2$ and 72.2%, 24.5% for 5%

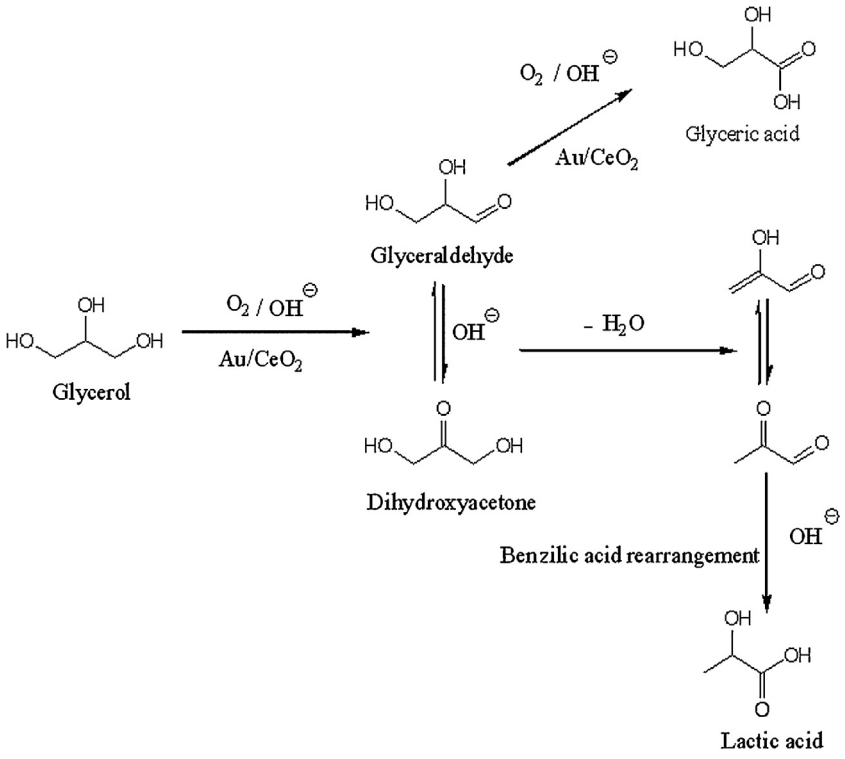


**Scheme 2.** Proposed reaction pathways of glycerol oxidation leading to glyceric and lactic acids.

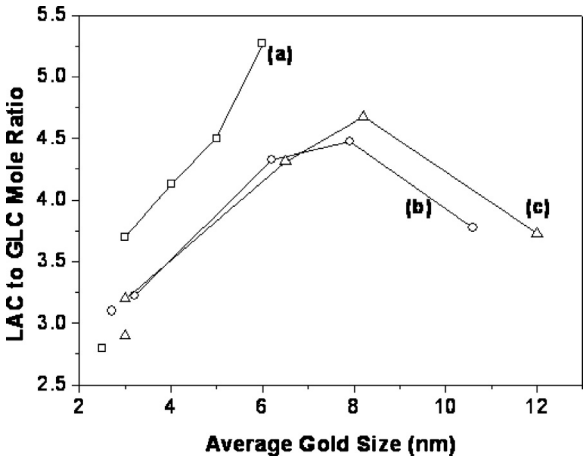


**Fig. 8.** Variation of lactic acid to glyceric acid mole ratio with catalyst to glycerol weight ratio during catalyst reduction. (a) 0.95% $Au/CeO_2$ (b) 2.74% $Au/CeO_2$ and (c) 4.59% $Au/CeO_2$–triangles. Reaction conditions: temperature of 90 °C, pressure of 1 atm under air with a flow rate of 0.15 L $min^{-1}$, and NaOH/glycerol = 4:1 (mole ratio).

$Au/CeO_2$). These results are consistent with the fact that, the gold particle size is roughly the same, whatever the gold loading (see the first lines (i) in the XRD patterns of Fig. 1a–c). Samples reduced under flowing hydrogen (300 °C/2 h) invariably produced small gold particles (<5 nm, invisible in the XRD analyses). In contrast, the chemically reduced samples exhibited gradually increasing average gold particle sizes due to the increasing catalyst/glycerol ratio during the reduction of the as-prepared catalysts (as seen by comparing the 1st XRD line in Fig. 2 with the other lines), which may influence the product distribution.

To elucidate the efficiency of gold catalysts toward the selective oxidation of glycerol to lactic acid, the product mole ratio of lactic acid to glyceric acid is plotted against the catalyst/glycerol weight ratio during the chemical reduction step (Fig. 8). As is evident from Fig. 8, increasing catalyst/glycerol ratio during the reduction of the gold catalysts leads to a progressive increase in the ratio of lactic acid to glyceric acid obtained with 1% $Au/CeO_2$ catalyst. In other words, as the average gold particle size increases, the selectivity to glyceric acid decreases and the selectivity to lactic acid increases. However, 3% and 5% $Au/CeO_2$ catalysts exhibit a volcano-shaped curve with maximum selectivity to lactic acid with medium-sized gold particles; both smaller and larger gold particles show inferior selectivity. Interestingly, the fall in selectivity to glyceric acid does not increase the selectivity to the other acid products that are derived from glyceric acid oxidation except lactic acid [26]. This observation correlates with literature reports [26,33–36] and suggests that the increased selectivity to lactic acid could be related to decreased activity of catalysts with larger gold particle sizes toward glycerol to glyceric acid oxidation. The catalytic results of the present study closely resemble those of Baiker et al. [36]. As the Au particle size of 1% $Au/CeO_2$ increases, the selectivity to lactic acid increases to a maximum level. In 3% and 5% $Au/CeO_2$ samples, optimum selectivity was obtained with a medium particle size, and smaller and larger gold particles lead to lower lactic acid selectivity. According to Davis et al., the selective oxidation of glycerol in the aqueous phase (with base) with supported gold catalysts proceeds through a reaction path that involves both solution-mediated (basic) and metal- (i.e., gold-) catalyzed steps [53]. In the present study, the metal-catalyzed aspect is considered separately (by maintaining the same basicity of the solution), which enables the effect of the average gold particle size to be determined. The decreasing selectivity to glyceric acid with increasing average gold particle size is also in agreement with the literature reports

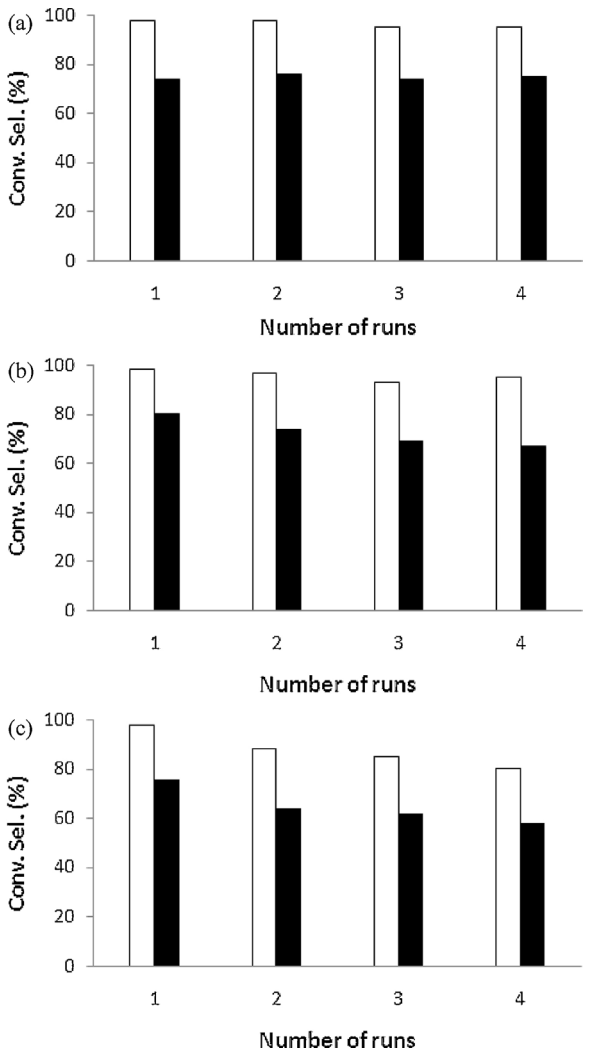


**Fig. 9.** Reusability results of (a) 0.95% $Au/CeO_2$, (b) 2.74% $Au/CeO_2$, (c) 4.59% $Au/CeO_2$ (catalyst to glycerol weight ratios of 0.005, 0.02 and 0.02, respectively). Reaction conditions: temperature of 90 °C, pressure of 1 atm under air with a flow rate of 0.15 L $min^{-1}$, and NaOH/glycerol = 4:1 (mole ratio).

[26,33–36,49–52]. Accordingly, the increase in the selectivity to lactic acid may be explained by the solution-mediated aspect of the catalysis, i.e., lactic acid selectivity could be more related to the base-catalyzed steps of the reaction (Scheme 2).

The glycerol oxidation pathways that lead to glyceric and lactic acids are different [32]. According to Liu et al., the formation of glyceric acid involves the gold-catalyzed transformation of glycerol into glyceraldehyde and dihydroxyacetone as intermediates and further gold-catalyzed oxidation of these intermediates to glyceric acid [32]. In contrast, the formation of lactic acid from the glyceraldehyde and dihydroxyacetone intermediates proceeds through base-catalyzed benzilic acid rearrangement and does not appear to involve the gold catalyst. Hence, the gold particle size is expected to have a more significant effect on glyceric acid formation than on lactic acid formation. Literature reports have shown that the catalytic activity decreases with increasing gold particle size for glycerol to glyceric acid oxidation. The present study shows that the glyceric acid selectivity also decreases with increasing gold particle size. In other words, as the decreased activity of catalysts with larger gold particles toward the conversion of glyceraldehydes and dihydroxyacetone into glyceric acid may facilitate base-catalyzed benzilic acid rearrangement to lactic acid since the reaction mixture contains four equivalents of base (in the present study). Thus,

these catalytic results show that lactic acid can be efficiently produced from glycerol using $Au/CeO_2$ catalysts containing suitably sized gold particles. Furthermore, the capacity of glycerol to act as a reducing agent enables the synthesis of $Au/CeO_2$ catalysts with larger gold particles; this presents a single-reagent method of controlling the size of ceria-supported gold particles. Thus, the prepared gold nanoparticles exhibit unprecedented catalytic activity toward the selective oxidation of glycerol at atmospheric pressure.

The performance of glycerol-reduced catalysts in reusability tests is presented in Fig. 9. The 1% $Au/CeO_2$ catalyst (reduced with a catalyst/glycerol ratio of 0.005, Fig. 9a) shows quite stable conversion and lactate selectivity during the reusability tests. The results obtained for 3% $Au/CeO_2$ (Fig. 9b) shows that the lactate selectivity decreases gradually with the number of cycles: A fall in the lactate selectivity from 74% to 58% was accompanied with decreasing conversion from 98% to 80% after four successive runs. To assess gold leaching, aliquots of the reaction mixture were analyzed with inductively coupled plasma atomic emission spectroscopy (ICPAES) after each run. The results showed no detectable leaching of gold, which demonstrates the stability of $Au/CeO_2$ samples against leaching during the catalytic reactions.

## 4. Conclusions

For the first time, the catalytic activity of ceria-supported gold nanoparticle catalysts prepared by chemical reduction with glycerol toward the selective aerobic oxidation of glycerol to lactic acid was explored. The results were compared with those of conventional hydrogen-reduced samples. The glycerol-based chemical reduction method not only enables the synthesis of larger gold particles (compared with hydrogen-reduced samples) on a nanosized ceria support, but also allows variation of the average gold particle sizes with fixed gold loading and without the need for other reagents. The catalyst/glycerol weight ratio affects the average gold particle size and, hence, the product distribution. This study reveals that $Au/CeO_2$ catalysts can efficiently catalyze the selective oxidation of glycerol to lactic acid at atmospheric pressure with higher selectivity to lactic acid than hydrogen-reduced samples.

## Acknowledgments

This work was supported by the Institutional Research Program (SI-1301) and partially funded by Korea Research Council for Industrial Science & Technology (ISTK, SK-1311). P. L. acknowledges Korea Research Institute of Chemical Technology (KRICT) for financial support through a post-doctoral program. Authors would like to thank to Prof. Harold H. Kung for his wonderful discussion.

## Appendix A. Supplementary data

Supplementary data associated with this article can be found, in the online version, at http://dx.doi.org/10.1016/j.apcata.2013.08.048.

## References

[1] S. Ebnesajjad, Handbook of Biopolymers and Biodegradable Plastics, Applied Science Publishers, 2012.
[2] P.P. Upare, Y.K. Hwang, J.S. Chang, D.W. Hwang, Ind. Eng. Chem. Res. 51 (2012) 4837–4842;
Y. Fan, C. Zhou, X. Zhu, Catal. Rev. Sci. Eng. 51 (2009) 293–324.
[3] R.M. West, M.S. Holm, S. Saravanamurugan, J. Xiong, Z. Beversdorf, E. Taarning, C.H. Christensen, J. Catal. 269 (2010) 122–130.
[4] J. Lunt, Polym. Degrad. Stab. 59 (1998) 145–152.
[5] K. Fukushima, Y. Kimura, Polym. Int. 55 (2006) 626–642.
[6] H. Kimura, K. Tsuto, T. Wakisaka, Y. Kazumi, Y. Inaya, Appl. Catal. A: Gen. 96 (1993) 217–228.
[7] A. Abbadi, H.V. Bekkum, Appl. Catal. A: Gen. 148 (1996) 113–122.
[8] R. Garcia, M. Besson, P. Gallezot, Appl. Catal. A: Gen. 127 (1995) 165–176.
[9] D.I. Enache, D. Barker, J.K. Edwards, S.H. Taylor, D.W. Knight, A.F. Carley, G.J. Hutchings, Catal. Today 122 (2007) 407–411.
[10] A. Abad, C. Almela, A. Corma, H. Garcia, Chem. Commun. (2006) 3178–3180.
[11] T. Mallat, A. Baiker, Chem. Rev. 104 (2004) 3037–3058.
[12] S. Carrettin, P. McMorn, P. Johnston, K. Griffin, G.J. Hutchings, Chem. Commun. (2002) 696–697.
[13] S. Carrettin, P. McMorn, P. Johnston, K. Griffin, C.J. Kiely, G.A. Attard, G.J. Hutchings, Top. Catal. 27 (2004) 131–136.
[14] S. Carrettin, P. McMorn, P. Johnston, K. Griffin, C.J. Kiely, G.J. Hutchings, Phys. Chem. Chem. Phys. 5 (2003) 1329–1336.
[15] I.H. Kishida, F. Jin, Z. Zhou, T. Moriya, H. Enomoto, Chem. Lett. 34 (2005) 1560–1562.
[16] D. Roy, B. Subramaniam, R.V. Chaudhari, ACS Catal. 1 (2011) 548–551.
[17] C.A. Ramirez-Lopez, J.R. Ochoa-Gomez, M. Fernandez-Santos, O. Gomez-Jimenez-Aberasturi, A. Alonso-Vicario, J. Torrecilla-Sori, Ind. Eng. Chem. Res. 49 (2010) 6270–6278.
[18] E.P. Maris, R.J. Davis, J. Catal. 249 (2007) 237–328.
[19] E.P. Maris, W.C. Ketchie, M. Murayama, R.J. Davis, J. Catal. 251 (2007) 281–294.
[20] J.C. Sowden, E.K. Pohlen, J. Am. Chem. Soc. 80 (1958) 242–244.
[21] G. Machell, G.N. Richards, J. Chem. Soc. (1960) 1924–1931.
[22] W.C. Ketchie, M. Murayama, R.J. Davis, J. Catal. 250 (2007) 264–273.
[23] P. Gallezot, Catal. Today 37 (1997) 405–418.
[24] M. Besson, P. Gallezot, Catal. Today 57 (2000) 127–141.
[25] F. Porta, L. Prati, J. Catal. 224 (2004) 397–403.
[26] C.L. Bianchi, P. Canton, N. Dimitratos, F. Porta, L. Prati, Catal. Today 102–103 (2005) 203–212.
[27] N. Dimitratos, C. Messi, F. Porta, L. Prati, A. Villa, J. Mol. Catal. A:Chem. 256 (2006) 21–28.
[28] S. Demirel-Glen, M. Lucas, P. Claus, Catal. Today 102–103 (2005) 166–172.
[29] S. Demirel, K. Lehnert, M. Lucas, P. Claus, Appl. Catal. B: Environ. 70 (2007) 637–643.
[30] S. Hirasawa, H. Watanabe, T. Kizuka, Y. Nakagawa, K. Tomishige, J. Catal. 300 (2013) 205–216.
[31] M. Checa, F. Auneau, J. Hidalgo-Carrillo, A. Marinas, J.M. Marinas, C. Pinel, F.J. Urbano, Catal. Today 196 (2012) 91–100.
[32] Y. Shen, S. Zhang, H. Li, Y. Ren, H. Liu, Chem. Eur. J. 16 (2010) 7368–7371.
[33] C. Bianchi, F. Porta, L. Prati, M. Rossi, Top. Catal. 13 (2000) 231–236.
[34] A. Villa, C.E. Chan-Thaw, L. Prati, Appl. Catal. B: Environ. 96 (2010) 541–547.
[35] N. Dimitratos, J.A. Lopez-Sanchez, D. Lennon, F. Porta, L. Prati, A. Villa, Catal. Lett. 108 (2006) 147–153.
[36] P. Haider, B. Kimmerle, F. Krumeich, W. Kleist, J.D. Grunwaldt, A. Baiker, Catal. Lett. 125 (2008) 169–176.
[37] L. Delannoy, K. Fajerwerg, P. Lakshmanan, C. Potvin, C. Methivier, C. Louis, Appl. Catal. B: Environ. 94 (2010) 117–124.
[38] Q. Fu, S. Kudriavtseva, H. Saltsburg, M.F. Stephanopoulos, Chem. Eng. J. 93 (2003) 41–53.
[39] J.J. Storhoff, A.A. Lazarides, R.C. Mucic, C.A. Mirkin, R.L. Letsinger, G.C. Schats, J. Am. Chem. Soc. 122 (2000) 4640–4650.
[40] R.R. Reynolds, C.A. Mirkin, R.L. Letsinger, J. Am. Chem. Soc. 122 (2000) 3795–3796.
[41] M. Sastry, N. Lala, V. Patil, S.P. Chavan, A.G. Chittiboyina, Langmuir 14 (1998) 4138–4242.
[42] R. Elghanian, J.J. Starhoff, R.C. Mucic, R.L. Letsinger, C.A. Mirkin, Science 277 (1997) 1078–1081.
[43] Y. Borensztein, L. Delannoy, A. Djedidi, R.G. Barrera, C. Louis, J. Phys. Chem. C 114 (2010) 9008–9021.
[44] L.D. Landau, E.M. Lifshitz, Electrodynamic of Continuous Media, Pergamon Press, New York, 1960.
[45] U. Kreibig, M. Vollmer, Optical Properties of Metal Clusters, Springer, New York, 1994.
[46] B. Palpant, B. Prevel, J. Lerme, E. Cottancin, M. Pellarin, M. Treilleux, A. Perez, J.L. Vialle, M. Broyer, Phys. Rev. B 57 (1998) 1963–1970.
[47] V. Myroshnychenko, J. Rodriguez-Fernandez, I. Pastoriza-Santos, A. Funston, M.C. Novo, P. Mulvaney, L.M. Liz-Marzan, F.J.G. De Abajo, Chem. Soc. Rev. 37 (2008) 1792–1805.
[48] C.G. Blatchford, J.R. Campbell, J.A. Creighton, Surf. Sci. 120 (1982) 435–455.
[49] N. Dimitratos, J.A. Lopez-Sanchez, G.J. Hutchings, Top. Catal. 52 (2009) 258–268.
[50] L. Prati, M. Rossi, J. Catal. 176 (1998) 552–560.
[51] F. Porta, L. Prati, M. Rossi, S. Colluccia, G. Martra, Catal. Today 60 (2000) 165–172.
[52] L. Prati, G. Martra, Gold Bull. 32 (1999) 96–101.
[53] B.N. Zope, D.D. Hibbitts, M. Neurock, R.J. Davis, Science 330 (2010) 74–78.